Universal coupling between metal-clad waveguides and optical ring resonators

Ian M. White, Jonathan D. Suter, Hesam Oveys, Xudong Fan

Department of Biological Engineering, University of Missouri-Columbia
240D Life Sciences Center, 1201 E. Rollins St. Columbia, MO 65211
fanxud@missouri.edu

Terry L. Smith, Junying Zhang, Barry J. Koch, and Michael A. Haase

Corporate Research Materials Laboratories, 3M Company
St. Paul, MN 55144-1000

Abstract: We demonstrate excitation of whispering gallery modes in optical ring resonators using a gold-clad pedestal planar waveguide structure. The gold-clad structure provides a strong evanescent field for light-coupling into the resonator while enabling low transmission loss throughout much of the visible and near-infrared region. This is advantageous compared to the previously demonstrated anti-resonant reflecting optical waveguide (ARROW) structure, which can only transmit a narrow wavelength band. We show that the height of the pedestal waveguide can be designed to optimize the coupling conditions for the ring resonator. This technology enhances the practicality of optical ring resonators for sensing devices, laser systems, and many other important applications.

©2007 Optical Society of America

OCIS codes: 230.7380, 230.5750, 300.6320, 290.4020, 170.4520

References and links

1. H. -M. Tzeng, K. F. Wall, and M. B. Long, "Laser emission from individual droplets at wavelengths corresponding to morphology-dependent resonances," Opt. Lett. **9**, 499-501 (1984).
2. M. Cai, O. Painter, K. J. Vahala, and P. C. Sercel, "Fiber-coupled microsphere laser," Opt. Lett. **25**, 1430-1432 (2000).
3. R. K. Chang and A. J. Campillo, eds., *Optical Processes in Microcavities* (World Scientific, Singapore, 1996).
4. K. Vahala, ed., *Optical Microcavities* (World Scientific, Singapore, 2005).
5. F. Vollmer, D. Braun, A. Libchaber, M. Khoshsima, I. Teraoka, and S. Arnold, "Protein detection by optical shift of a resonant microcavity," Appl. Phys. Lett. **80**, 4057-4059 (2002).
6. I. M. White, N. M. Hanumegowda, and X. Fan, "Subfemtomole detection of small molecules with microsphere sensors," Opt. Lett. **30**, 3189-3191 (2005).
7. N. M. Hanumegowda, C. J. Stica, B. C. Patel, I. M. White, and X. Fan, "Refractometric sensors based on microsphere resonators," Appl. Phys. Lett. **87**, 201107 (2005).
8. N. M. Hanumegowda, I. M. White, and X. Fan, "Aqueous mercuric ion detection with microsphere optical ring resonator sensors," Sens. Actuators B **120**, 207-212 (2006).
9. A. Yalcin, K. C. Popat, J. C. Aldridge, T. A. Desai, J. Hryniewicz, N. Chbouki, B. E. Little, O. King, V. Van, S. Chu, D. Gill, M. Anthes-Washburn, M. S. Unlu, and B. B. Goldberg, "Optical Sensing of Biomolecules Using Microring Resonators," IEEE J. Sel. Top. Quantum Electron. **12**, 148-155 (2006).
10. C. F. Bohren and D. R. Huffman, *Absorption and Scattering of Light by Small Particles* (John Wiley & Sons, Inc., New York, 1998).
11. M. L. Gorodetsky and V. S. Ilchenko, "High-Q optical whispering-gallery microresonators: precession approach for spherical mode analysis and emission patterns with prism couplers," Opt. Commun. **113**, 133-143 (1994).
12. V. S. Ilchenko, X. S. Yao, and L. Maleki, "Pigtailing the high-Q microsphere cavity: a simple fiber coupler for optical whispering-gallery modes," Opt. Lett. **24**, 723-725 (1999).
13. B. E. Little, J. -P. Laine, D. R. Lim, H. A. Haus, L. C. Kimerling, and S. T. Chu, "Pedestal antiresonant reflecting waveguides for robust coupling to microsphere resonators and for microphotonic circuits," Opt. Lett. **25**, 73-75 (2000).

#78139 - $15.00 USD Received 15 December 2006; revised 11 January 2007; accepted 13 January 2007
(C) 2007 OSA

14. I. M. White, H. Oveys, X. Fan, T. L. Smith, and J. Zhang, "Integrated multiplexed biosensors based on liquid core optical ring resonators and antiresonant reflecting optical waveguides," Appl. Phys. Lett. **89**, 191106 (2006).
15. J. R. Feth and C. L. Chang, "Metal-clad fiber-optic cutoff polarizer," Opt. Lett. **11**, 386-388 (1986).
16. M. Zourob, S. Mohr, B. J. Treves Brown, P. R. Fielden, M. McDonnell, and N. J. Goddard, "The development of a metal clad leaky waveguide sensor for the detection of particles," Sens. Actuators B **90**, 296–307 (2003).
17. N. Skivesen, R. Horvath, and H. C. Pedersen, "Peak-type and dip-type metal-clad waveguide sensing," Opt. Lett. **30**, 1659-1661 (2005).
18. M. A. Duguay, Y. Kokubun, T. L. Koch, and Loren Pfeiffer, "Antiresonant reflecting optical waveguides in SiO_2-Si multilayer structures," Appl. Phys. Lett. **49**, 13-15 (1986).
19. T. Baba, Y. Kokubun, T. Sakaki, and K. Iga, "Loss Reduction of an ARROW Waveguide in Shorter Wavelength and Its Stack Configuration," J. Lightwave Technol. **6**, 1440 - 1445 (1988).
20. M. Born and E. Wolf, *Principles of Optics* (Cambridge University Press, 1997).
21. D. R. Lide, ed., *Handbook of Chemistry and Physics* (CRC Press, 2005).
22. I. M. White, H. Oveys, and X. Fan, "Liquid-core optical ring-resonator sensors," Opt. Lett. **31**, 1319-1321 (2006).
23. M. L. Gorodetsky and V. S. Ilchenko, "Optical microsphere resonators: optimal coupling to high-*Q* whispering-gallery modes," J. Opt. Soc. Am. B **16**, 147-155 (1999).
24. M. Noto, F. Vollmer, D. Keng, I. Teraoka, and S. Arnold, "Nanolayer characterization through wavelength multiplexing of a microsphere resonator," Opt. Lett. **30**, 510-512 (2005).

1. Introduction

Optical ring resonators have been heavily studied for a number of applications, including lasers [1, 2], cavity quantum electrodynamics [3, 4], optical filters [4], and bio/chemical sensors [5-9]. These ring-, disk-, or sphere-shaped dielectrics act as a resonating cavity for light of wavelengths that match the resonance condition. These resonating optical modes are referred to as whispering gallery modes (WGMs) [3, 4, 10]. Due to the extremely high Q-factor of the WGMs in optical ring resonators (10^6 to 10^9 for microspheres [8, 11]), photons may circulate the cavity thousands of times or more, resulting in a strong localized field enhancement and, in the case of sensors, excellent light-matter interaction.

Excitation of the WGMs has been achieved using free space coupling [1], optical fiber tapers [2], prism [11], and angle-cleaved/polished fiber [8, 12], with the coupling efficiency ranging from a few percent to 100% (critical coupling). These excitation techniques are sufficient for laboratory settings. However, for the purposes of integration, miniaturization, and robustness, a planar waveguide is necessary to deliver the light to the ring resonator. Recently, the anti-resonant reflecting optical waveguide (ARROW) structure has been employed for the excitation of WGMs in microspheres [13] and in cylindrical ring resonators [14]. This structure prevents leakage into the substrate while presenting a sufficient evanescent field for the coupling between the waveguide and the ring resonator. Although these demonstrations accomplish the goal of a miniaturized and robust configuration, the ARROW structure is highly wavelength dependent because it relies on the resonant nature of reflections from multiple dielectric layers in the cladding. As a result, the ARROW planar waveguide is only effective for a specific wavelength region.

In this work, we investigate the excitation of WGMs in ring resonators utilizing a simple structure based on a gold-clad planar waveguide, as illustrated in Fig. 1. Similar structures have been used for a polarizer [15] and sensing [16, 17]. A thin gold cladding layer acts as a

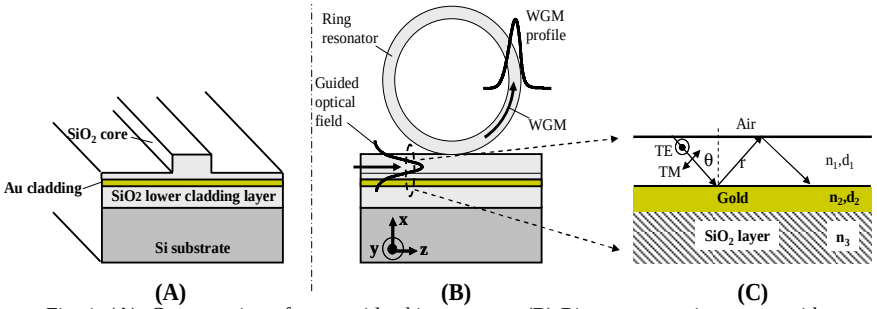


Fig. 1. (A). Cross-section of waveguide chip structure. (B) Ring resonator in contact with waveguide for WGM excitation. (C) Propagation of light along the waveguide, as it reflects off of the gold layer.

#78139 - $15.00 USD Received 15 December 2006; revised 11 January 2007; accepted 13 January 2007
(C) 2007 OSA

mirror that prevents light leakage into the substrate over a large range of wavelengths. Meanwhile, a high evanescent field is presented at the top of the waveguide for sufficient excitation of the ring resonator WGMs. In this paper, we analyze the transmission and coupling characteristics of the gold-clad waveguide, and we experimentally demonstrate efficient WGM excitation in both microsphere and cylindrical resonators at wavelengths of 690 nm, 980 nm and 1550 nm.

2. Theory

2.1 Transmission loss

The wavelength dependent loss for both the gold-clad waveguide and the ARROW can be calculated using simple ray optics while considering the light reflections during propagation at the interface between the waveguide core and gold cladding. Assuming that the waveguide core height is large compared to the wavelength in the core, the incident reflection angle θ for the fundamental mode can be approximated as $\cos(\theta) = \lambda/(2n_1d_1)$ [18,19], where λ is the wavelength in vacuum, n_1 is the waveguide core refractive index, and d_1 is the waveguide core height. This is illustrated in Fig. 1(C). The reflection coefficient for the incident wave is [20]:

$$r = \frac{r_{12} + r_{23}\exp(2ik_{z2}d_2)}{1 + r_{12}r_{23}\exp(2ik_{z2}d_2)}, \tag{1}$$

where r_{12} and r_{23} are the reflection coefficients at the interfaces of the waveguide core and gold cladding and the gold cladding and silica substrate, respectively, and d_2 is the thickness of the gold cladding layer. These reflections can be expressed in a general form:

$$r_{mn} = \frac{Z_m - Z_n}{Z_m + Z_n} \qquad (m,n = 1,2,3). \tag{2}$$

For TE (TM) polarized waves, $Z_m = k_{zm}$ (ε_m/k_{zm}), where $k_{zm} = \sqrt{\varepsilon_m k_0^2 - k_1^2}$, $k_0 = 2\pi/\lambda$ and $k_1 = \sqrt{\varepsilon_1}k_0\sin(\theta)$. ε_m is the dielectric constant.

Since the light undergoes total internal reflection at the interface between the core and the air, the transmission loss is solely determined by the loss due to the leakage into the substrate and the absorption of the gold [19]:

$$Loss(dB) = -10\log(|r|^{2N}) = -20N\log|r|, \tag{3}$$

where N is the number of reflections along a given transmission distance, assuming that the distance between reflections is $2d_1\tan(\theta)$.

The wavelength dependent loss for the gold-clad waveguide is plotted in Fig. 2(A) for TE and TM polarizations and waveguide core heights of 2 μm and 2.5 μm. For these calculations, the silica waveguide core and lower cladding are assumed to have a refractive index of 1.46, while the gold layer wavelength-dependent refractive index, and thus ε_2, are taken from [21]. For the TE mode, the loss is well below 1 dB/cm for the entire wavelength range between 0.6 μm and 2 μm. The TM mode suffers higher loss, but is still less than 10 dB/cm for this wavelength range.

For comparison, the wavelength-dependent loss for an ARROW structure designed to transmit 980 nm light is shown in Fig. 2(B). Instead of the gold cladding layer, the ARROW structure uses alternating layers of high and low refractive index as a reflective lower cladding [18,19]. The calculations are based on a high refractive index layer of SiN (184 nm, n = 2.0) and a low refractive index layer of SiO_2 (n = 1.45), as described in [14]. This ARROW has a loss below 10 dB/cm over a range of about 0.6 μm to 1 μm, but has much higher loss at higher wavelengths. The minimum loss can be reduced by utilizing more reflecting layers, but the wavelength dependent shape is an inherent property of ARROWs. In fact, utilizing more reflecting layers decreases the spectral width of the low-loss region [20].

#78139 - $15.00 USD Received 15 December 2006; revised 11 January 2007; accepted 13 January 2007
(C) 2007 OSA

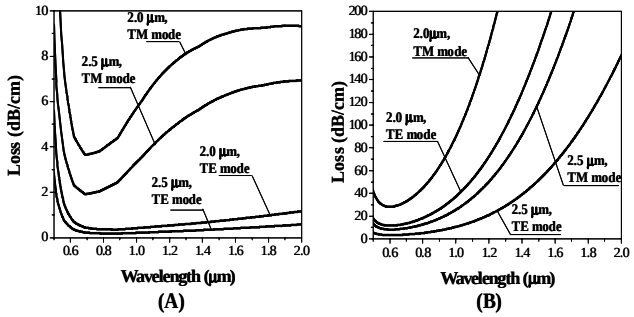


Fig. 2. (A). Wavelength dependent transmission loss for a gold-clad waveguide of heights 2.0 and 2.5 μm. Gold layer thickness: 300 nm. (B). Wavelength dependent transmission loss for an ARROW of heights 2.0 and 2.5 μm.

2.2 Mode coupling

In addition to the low transmission loss, the gold-clad waveguide structure also provides a strong evanescent field for coupling into the ring resonator. The coupling between the waveguide and the ring resonator is based on frustrated total internal reflection, and is governed by the overlap between the evanescent fields at the surface of the two objects. The calculated field distributions for a waveguide height of 2 μm and a cylindrical ring resonator [orientation shown in Fig. 1(B)] with a diameter of 100 μm are shown in Fig. 3(A). The waveguide mode is calculated using the typical boundary condition analysis. As an approximation, the electric field is set to zero at the interface between the waveguide core and the gold cladding layer due to the gold's strong reflectivity. The WGM of the cylindrical ring resonator is computed using a tool developed in-house based on Mie theory, as described previously [22].

To theoretically assess the coupling between the gold-clad waveguide and a cylindrical resonator, we calculate the coupling coefficient at 690 nm, 980 nm, and 1550 nm. The single-trip coupling coefficient κ^2 is related to the product of the mode fields of the metal-clad waveguide and cylindrical ring resonator, *i.e*,

$$\kappa^2 = \left\{ \frac{2\pi R}{\gamma} \exp\left[\frac{(\Delta\beta)^2 R}{\gamma} \right] \right\} \frac{k^4}{4\beta_{RR}\beta_{WG}} \left(n_{RR}^2 - n_0^2\right)\left(n_{WG}^2 - n_0^2\right) \int_{RR} e_{RR} e_{WG}\, dx \int_{WG} e_{RR} e_{WG}\, dx \cdot \qquad (4)$$

The subscripts *RR* and *WG* refer to the ring resonator and the waveguide, respectively. The term k is equal to $2\pi/\lambda$, n is the refractive index, and β is the propagation constant in the respective material. For the ring resonator, β_{RR} is approximated as ℓ/R, where ℓ is the angular momentum term and R is the outer radius. For the waveguide, $\beta_{WG} \approx \sqrt{(n_{WG}k)^2 - (\pi/h)^2}$, where h is the height of the waveguide core [14]. The guided modes in the ring resonator and the waveguide are described by e_{RR} and e_{WG}, respectively, where both fields are normalized to their respective total intensity in the *x-y* plane. The subscript *RR (WG)* on the integral indicates that the integration takes place in the ring resonator (waveguide). $\Delta\beta$ is the propagation constant mismatch between the ring resonator and the waveguide and γ is the decay constant of the ring resonator evanescent field, approximated as $k\sqrt{n_{RR}^2 - 1}$.

The coupling coefficient is plotted in Fig. 3(B) for 690 nm, 980 nm, and 1550 nm and for waveguide heights ranging between 2 μm and 4 μm. A logarithmic plot is used to demonstrate less than a factor of 100 difference between the highest coupling at 1550 nm and the lowest at 690 nm. The fractional depth of the resonance K is related to κ^2 by $K = (4Q_cQ_0)/(Q_c+Q_0)^2$, where Q_c is the coupling Q-factor and inversely proportional to κ^2, and Q_0 is the ring

#78139 - $15.00 USD Received 15 December 2006; revised 11 January 2007; accepted 13 January 2007
(C) 2007 OSA

resonator intrinsic Q-factor [23]. Fig. 3(C) shows that a high degree of coupling can be achieved over two orders of magnitude of variation among Q_c centered around Q_0. Therefore, it is expected that effective coupling can be achieved for all three wavelengths based on the relatively small range of variation in κ^2 shown in Fig. 3(B).

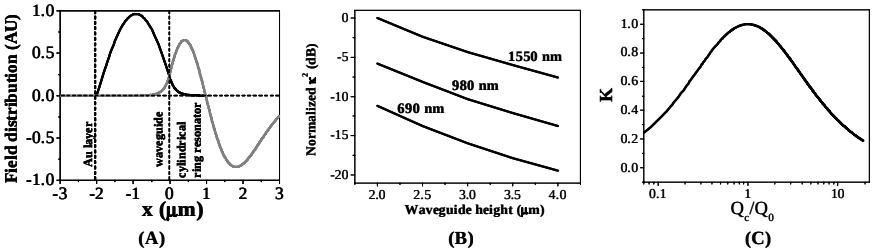


Fig. 3. (A). Mode profiles of the light propagating along the waveguide and the 2nd order radial WGM in a cylindrical ring resonator. Ring resonator diameter: 100 μm. (B.) Single-trip coupling coefficient normalized to the 1550 nm excitation from a 2 μm waveguide.

3. Experimental demonstration

The gold-clad waveguide chip is fabricated by depositing a 3-5 μm SiO_2 lower cladding onto a silicon wafer by plasma enhanced chemical vapor deposition (PECVD). Then, a 300 nm gold layer is deposited by electron beam evaporation. The SiO_2 waveguide core layer is then created by PECVD growth on top of the gold. The thickness of this layer is varied in order to achieve different coupling efficiencies between the optical ring resonator and the waveguide. Next, the waveguide core layer is coated with aluminum by conventional techniques, including sputtering, evaporation and electron beam evaporation. A positive photoresist is coated on the aluminum layer, which is patterned using a mask and standard photolithography techniques. The patterned aluminum layer defines the positions of the pedestal waveguides, which are 5 μm wide. Reactive ion etching is performed to etch the SiO_2 layer and form pedestal waveguide cores. Finally, aluminum is removed through a wet etch.

To demonstrate the broad wavelength range of the gold-clad waveguides, we simultaneously excite WGMs in a cylindrical ring resonator of 140 μm in diameter at 690 nm and 1550 nm. The experimental setup is presented in Fig. 4. Light from a 690 nm tunable diode laser is combined with light from a 1550 nm tunable diode laser onto a fiber cable using an optical coupler. Both lasers are scanned periodically across a range of approximately 100 pm. Both signals are then coupled into the waveguide, where they excite WGMs in a cylindrical resonator that is placed in contact the waveguide. The optical signals are collected at the output of the waveguide. Dips in the spectral traces indicate that the laser light has coupled into the WGMs. To separate the signals during detection, one of the two lasers is turned off during the signal acquisition.

WGMs recorded for both wavelengths are shown in Fig. 5(A), along with Lorentzian line-fits for the two modes. The coupling is higher at the 1550 nm wavelength, indicating

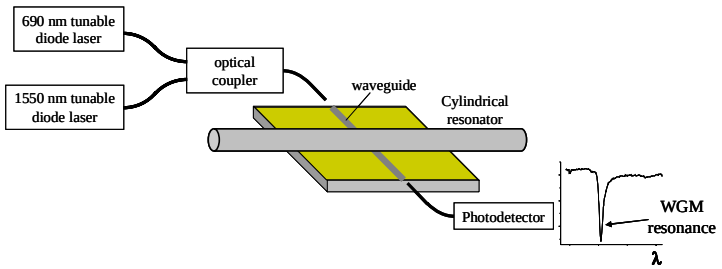


Fig. 4. Experimental setup to excite WGMs in a cylindrical ring resonator using both 690 nm and 1550 nm light.

#78139 - $15.00 USD Received 15 December 2006; revised 11 January 2007; accepted 13 January 2007
(C) 2007 OSA

operation in the under-coupling regime [23]. The Q-factor, which is defined as the wavelength divided by the full-width at half-max linewidth, is 5.3×10^5 for the 690 nm WGM, and 3.3×10^5 for the 1550 nm WGM.

To further demonstrate the applicability of the gold-clad waveguide, we then repeated the experiment using an optical microsphere ring resonator and a waveguide of 2 μm in height. WGMs recorded for wavelengths of 690 nm, 980 nm, and 1550 nm are presented in Fig. 5(B). Just as with the cylindrical resonator, higher wavelengths result in higher coupling. The Q-factor for the 690 nm WGM is 6.8×10^5, while the 1550 nm WGM has a Q-factor of 6.7×10^5.

As shown in Fig. 3, the coupling between the waveguide and ring resonator can be adjusted by changing the waveguide height. Using the experimental setup shown in Fig. 4, we recorded WGMs that are excited using waveguides of heights of 2 μm, 2.5 μm, and 3 μm. Only the 1550 nm laser is used for mode excitation. Lorentzian fits of the recorded modes are shown in Fig. 6. With the 3.0 μm waveguide, the coupling is only approximately 20%, while the coupling is around 50% for the 2.0 μm waveguide, which confirms that the waveguide and ring resonator are in the under-coupling regime [23].

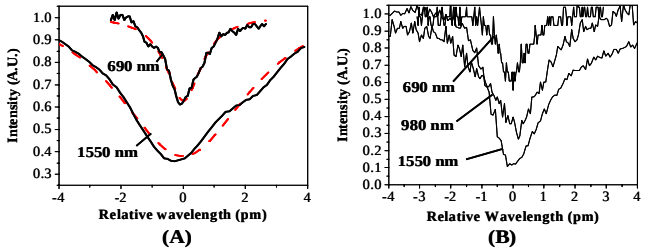


Fig. 5. (A). WGMs in a cylindrical resonator of 140 μm in diameter for 690 nm and 1550 nm that are excited by a gold-clad waveguide of 2.5 μm in height. (B) WGMs in a microsphere of 180 μm in diameter for 690 nm, 980 nm, and 1550

4. Conclusion

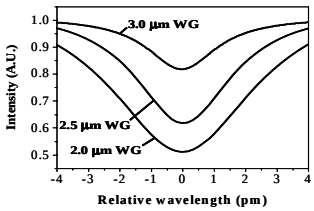


Fig. 6. Lorentzian fits of recorded WGMs in cylindrical resonators excited by 1550 nm light coupled from gold-clad waveguides of heights of 2.0, 2.5, and 3.0 m.

We have demonstrated the use of metal-clad pedestal waveguides for excitation of WGMs in cylindrical and microsphere resonators over a broad wavelength range from 690 nm to 1550 nm. Such WGM excitation capability enables multi-wavelength sensitivity, which will be useful in several applications, including the simultaneous determination of both layer thickness and refractive index of an analyte layer, as was demonstrated with a fiber taper and microsphere by Noto, *et al*. in Ref [24]. Moreover, the utilization of the waveguide chip enables a robust implementation with the possibility of dense multiplexing.

Acknowledgments

The authors acknowledge the support from the 3M Non-Tenured Faculty Award, the Wallace H. Coulter Early Career Award, the MU Research Council, and the NIH Mentored Quantitative Research Career Development Award.